# AMERICAN METEOROLOGICAL SOCIETY
**AMS Journals Online**

## Full Text View

# The Generation of Large-Amplitude Unsteady Lee Waves by Subinertial $K_1$ Tidal Flow: A Possible Vertical Mixing Mechanism in the Kuril Straits

**Tomohiro Nakamura, Toshiyuki Awaji, Takaki Hatayama, and Kazunori Akitomo**

*Department of Geophysics, Kyoto University, Kyoto, Japan*

**Takatoshi Takizawa**

*Japan Marine Science and Technology Center, Yokosuka, Japan*

**Tokihiro Kono and Yasuhiro Kawasaki**

*Hokkaido National Fisheries Research Institute, Kushiro, Japan*

**Masao Fukasawa**

*School of Marine Science and Technology, University of Tokai, Shizuoka, Japan*

### ABSTRACT

Numerical experiments with a two-dimensional nonhydrostatic model are performed to investigate tidally generated internal waves in the Kuril Straits and their effect on vertical mixing. The results show that sill-scale internal waves at the $K_1$ tidal frequency are confined to the sill slopes because the $K_1$ tide is subinertial in the Kuril Straits. In contrast to previous theories, the authors show that intense short internal waves generated at the sill breaks by the subinertial $K_1$ tidal current can propagate upstream as the tidal current slackens. Theoretical considerations identify these short waves as unsteady lee waves, which tend to be trapped at the generation region and grow into large-amplitude waves, eventually inducing vigorous mixing along their ray paths. In particular, superposition of a propagating unsteady lee wave and a newly generated lee wave over a sill causes significant wave breaking leading to a maximum vertical diffusivity of $\sim 10^3$ cm$^2$ s$^{-1}$. This quite intense mixing reaches down to the density layer of the North Pacific Intermediate Water (NPIW). In contrast, the $M_2$ tidal current does not cause such strong vertical mixing, because most of generated internal waves propagate away as first-mode internal tides and because the barotropic flow amplitude is small. The authors therefore suggest the possibility that generation of lee waves through interactions between the $K_1$ current and the bottom topography of the Kuril Straits contributes to the observed modification of the Okhotsk Sea water required in the formation of the NPIW.

Options:
- Create Reference
- Email this Article
- Add to MyArchive
- Search AMS Glossary

Search CrossRef for:
- Articles Citing This Article

Search Google Scholar for:
- Tomohiro Nakamura
- Toshiyuki Awaji
- Takaki Hatayama

- Kazuhiro Akitomo
- Takatoshi Takizawa
- Tokihiro Kono
- Yasuhiro Kawasaki
- Masao Fukasawa

## 1. Introduction

In the Okhotsk Sea, subduction due to sea ice formation produces considerably low-salinity and recently ventilated water at intermediate depths, and sea ice melting freshens the surface layer (Kitani 1973; Ohtani 1989; Talley and Nagata 1991). Many studies have indicated that the outflow of such remarkably low-salinity water from the Okhotsk Sea plays an important role in the production of the North Pacific Intermediate Water (NPIW), which is characterized by a salinity minimum (Wüst 1930; Talley 1991; Kono 1996; Yasuda 1997). Since the density range of the NPIW ($\sim 26.8$ $\sigma_\theta$) does not outcrop in the open

North Pacific Ocean, a driving mechanism is required for downward motion of fresh subarctic surface water, which in turn may induce effective subduction of other materials such as carbon dioxide ($CO_2$). Since the NPIW is distributed in the entire

subtropical gyre and even extends to the Tropics (Talley 1993), the formation mechanism of the NPIW has important implications for the dynamics of the mid-depth circulation in the North Pacific and the sources and paths through which anomalies and materials in the surface layer are conveyed into the intermediate layer. Therefore, the interaction process between the Okhotsk Sea and the North Pacific needs to be clarified in order to better understand the circulation and water properties of the North Pacific intermediate layer.

To assess the impact of the Okhotsk Sea on the North Pacific, it is necessary to study the water modification process in the Kuril Straits in relation to the water exchange taking place between the two basins. Kitani (1973) showed that in the northern Okhotsk Sea, the freezing of fresh surface waters can form cold saline waters as dense as 27.05 $\sigma_\theta$, which still

have lower salinity than the ambient waters at the same density. Associating an analysis of historical hydrographic data with the Kitani (1973) result, Talley (1991) proposed that the North Pacific at mid-depth is ventilated through sea ice formation in the innermost part of the Okhotsk Sea. From potential vorticity maps, Talley (1993) and Yasuda et al. (1996) commented that the Okhotsk Sea supplies low salinity water to the NPIW. These conclusions were also supported by recent studies. Warner et al. (1996) showed that the Okhotsk Sea is an important location for the ventilation of the intermediate water of the North Pacific based on chlorofluorocarbon (CFC) observations. Yasuda (1997) and Watanabe and Wakatsuchi (1998) showed the presence of a pycnostad (i.e., low potential vorticity) at 26.8 $\sigma_\theta$ in the Okhotsk Sea and suggested that low

potential vorticity water flowing out into the North Pacific even determines the density of the NPIW. In this process, turbulence and mixing is considered to be driven by conversion of the relatively high potential energy of the outflowing water into kinetic energy.

However, questions still remain concerning the role of the Okhotsk Sea and its significance for the NPIW formation. Recent detailed observations across Bussol Strait (Kawasaki and Kono 1994), where most of the outflow from the Okhotsk Sea is considered to occur, have clearly revealed the presence of a deep vertically uniform temperature distribution, leading to a horizontal discontinuity in the temperature distribution around the sill region (Fig. 1 ⊙). These facts are more likely to be explained by vertical mixing produced by interactions between swift tidal currents and sill topography in the Kuril Straits and hence suggest the presence of tidal mixing as another possible mixing mechanism. In fact, several previous studies pointed to the importance of tidal mixing on the water modification in the Kuril Straits (e.g., Talley 1991). However, as the actual physical mechanisms are still unknown, further investigation of the mechanism of tidal mixing at the Kurils is necessary.

According to the observations, the currents are dominated by the diurnal tidal components in the Kuril Straits, and the semidiurnal components are rather weak (Thomson et al. 1997). Our numerical simulation of barotropic tides around the Kuril Straits shows that the $K_1$ tide is predominant and induces very swift currents of up to 1.5 m s$^{-1}$ (Nakamura et al.

2000). Such strong tidal currents have been thought to cause intense vertical mixing by interactions with the large amplitude sills in the Kuril Straits. However, this situation is out of the range of previous theories for the growth of oceanic internal waves, which assume that an oscillating tidal flow over an obstacle excites only internal waves at its tidal frequency (internal tides). Since the diurnal tides are subinertial around this high latitude ($\sim 47°$N), internal tides at the $K_1$ tidal frequency are not

freely propagating waves. This fact prevents us from using the model described by Hibiya (1986), which assumes that internal tides propagating upstream are trapped at the generation region and amplified when the barotropic flow is critical (i.e., when the Froude number $F_n$ is unity, where $F_n$ is the ratio of the barotropic tidal flow speed to phase speed of the $n$th

mode). For the same reason, interpretations of wave growth by the critical slope theory (e.g., Wunsch 1969) or the nonlinear steepening effect (e.g., Lee and Beardsley 1974; Gerkema and Zimmerman 1995) are also inapplicable.

Thus, as a first step toward clarifying the physics responsible for the vertical mixing in the Kuril Straits and its influence on the North Pacific intermediate layer, we have performed numerical simulations of tidally generated internal waves and their nonlinear evolution in the Kuril Straits, and have estimated the vertical mixing induced by those waves. Our work is primarily a modeling study of one possible mixing process. The relative importance of other processes (e.g., potential energy dissipation described above) will be assessed in later work. For simplicity, we use a two-dimensional nonhydrostatic $f$-plane model with realistic topography and stratification, because inclusion of the rotation effect is necessary to investigate the difference between the superinertial $M_2$ tide and the subinertial $K_1$ tide and because nonhydrostatic models can reproduce

shear instability and/or convective instability. The latter processes are important in vertical mixing induced by waves (Scinocca and Peltier 1993), thus making the use of a two-dimensional model meaningful, although it cannot fully reproduce mixing because mixing is indeed a three-dimensional process. We are therefore able to estimate the tidal mixing reasonably, which is a subgrid-scale process and is not properly taken into account in general circulation models.

The outline of this paper is as follows. In section 2, the numerical model and parameters used are described. The model results are presented in section 3 for the $M_2$ and $K_1$ cases. In section 4, the excitation mechanism of internal waves is investigated by focusing on the excitation of propagating lee waves by oscillating tidal currents over topography, and their subsequent evolution leading to wave breaking in the $K_1$ case in section 5. The vertical mixing induced by tidally generated internal waves is estimated in section 6, and the energetics of internal waves are discussed in section 7. Our conclusions are summarized and discussed in section 8.

## 2. Numerical model

The model bottom topography (Fig. 2 ⊙) is representative of the sills in the northeastern part of the Kuril Straits (in particular, the sill in Nadezhdy Strait), where strong tidal currents can cause considerable mixing. Although there are a variety of sill depths (ranging between tens to several thousands m) in the Kuril Straits, the present sill topography is of a basic form so that simulation results can be qualitatively applied to cover other cases. Recent observations reveal that both water exchange and mixing occur between the Okhotsk Sea and the North Pacific through the northeastern part of the Kuril Straits as the western boundary current of the subarctic gyre (the East Kamchatka Current) flows along the Kuril Islands (Kawasaki and Kono 1994; Kono and Kawasaki 1997). They also indicate that the water in Bussol Strait, considered to be the main path of the outflow, has already been subjected to strong vertical mixing in the northeastern part of the Kuril Straits. The sill topography is determined according to the DBDB5 topographic data (National Geophysical Data Center, Boulder, Colorado) with a minimum depth of 550 m at the sill top. The bottom topography on both sides of the sill is set to be flat with a maximum depth of 2000 m. We can adopt this flat bottom simplification since the density core of the NPIW ($\sigma_\theta \sim 26.8$) is around a depth of 300 m.

In order to simulate vertical mixing by internal waves, we used a nonhydrostatic model with horizontal and vertical grid sizes of 500 and 10 m, respectively. The eddy viscosity and diffusivity coefficients are assigned to the relatively small values of $2 \times 10^5$ cm$^2$ s$^{-1}$ horizontally and 0.1 cm$^2$ s$^{-1}$ vertically so that their effect on mixing is small enough to demonstrate the wave mixing clearly. As basic forcing terms for internal wave generation, barotropic $K_1$ and $M_2$ currents are given at both lateral boundaries. Their maximum speeds at the sill top are 0.5 m s$^{-1}$ for the $K_1$ case and 0.2 m s$^{-1}$ for the $M_2$ case, as determined from our preceding barotropic tidal simulations (details in the accompanying paper, Nakamura et al. 2000). We took account of the effect of rotation by adopting an $f$-plane approximation to distinguish the physics of waves generated by the subinertial $K_1$ flow from that by the superinertial $M_2$ flow in the Kuril Straits. Thus the governing equations of our two-dimensional model are

$$\frac{\partial u}{\partial t} + u\frac{\partial u}{\partial x} + w\frac{\partial u}{\partial z} - fv = -\frac{1}{\rho_0}\frac{\partial p}{\partial x} + \nu_H\frac{\partial^2 u}{\partial x^2}$$

$$+ \nu_Z\frac{\partial^2 u}{\partial z^2}, \tag{1}$$

$$\frac{\partial v}{\partial t} + u\frac{\partial v}{\partial x} + w\frac{\partial v}{\partial z} + fu = \nu_H\frac{\partial^2 v}{\partial x^2} + \nu_Z\frac{\partial^2 v}{\partial z^2}, \tag{2}$$

$$\frac{\partial w}{\partial t} + u\frac{\partial w}{\partial x} + w\frac{\partial w}{\partial z} = -\frac{1}{\rho_0}\frac{\partial p}{\partial z} - \frac{\rho}{\rho_0}g$$

$$+ \nu_H\frac{\partial^2 w}{\partial x^2} + \nu_Z\frac{\partial^2 w}{\partial z^2}, \tag{3}$$

$$\frac{\partial u}{\partial x} + \frac{\partial w}{\partial z} = 0, \tag{4}$$

$$\frac{\partial \theta}{\partial t} + u\frac{\partial \theta}{\partial x} + w\frac{\partial \theta}{\partial z} = \kappa_H\frac{\partial^2 \theta}{\partial x^2} + \kappa_Z\frac{\partial^2 \theta}{\partial z^2}, \tag{5}$$

$$\frac{\partial S}{\partial t} + u\frac{\partial S}{\partial x} + w\frac{\partial S}{\partial z} = \kappa_H\frac{\partial^2 S}{\partial x^2} + \kappa_Z\frac{\partial^2 S}{\partial z^2}, \tag{6}$$

$$\rho = \rho(\theta, S, p), \tag{7}$$

where $(x, y, z)$ are the across-sill, along-sill, and vertical coordinates, respectively; $(u, v, w)$ are the velocity in the $(x, y,$

$z$) directions; $p$ is pressure; $\rho$ is density variation; $\theta$ is potential temperature; $S$ is salinity; $f$ ($=1.07 \times 10^{-4}$ s$^{-1}$) is the Coriolis parameter at 47°N; $\rho_0$ is the reference density; $g$ is the gravity acceleration; and $\nu$ and $\kappa$ are the coefficients of eddy viscosity and eddy diffusivity, respectively, with the subscripts $H$ and $Z$ for the horizontal and vertical direction. The equation of state used is based on Bryan and Cox (1972). In performing the model calculation, we solve the vorticity equation derived from Eqs. (1) and (3) as

$$\frac{\partial \zeta}{\partial t} + u\frac{\partial \zeta}{\partial x} + w\frac{\partial \zeta}{\partial z} + f\frac{\partial v}{\partial z}$$

$$= -\frac{g}{\rho_0}\frac{\partial \rho}{\partial x} + \nu_H\frac{\partial^2 \zeta}{\partial x^2} + \nu_Z\frac{\partial^2 \zeta}{\partial z^2} \qquad (8)$$

and the Poisson equation for the stream function $\psi$ as

$$\frac{\partial^2 \psi}{\partial x^2} + \frac{\partial^2 \psi}{\partial z^2} = \zeta, \qquad (9)$$

where the relative vorticity $\zeta$ and the streamfunction $\psi$ are defined, respectively, as

$$\zeta = \frac{\partial w}{\partial x} - \frac{\partial u}{\partial z}, \qquad (10)$$

$$u = -\frac{\partial \psi}{\partial z}, \qquad w = \frac{\partial \psi}{\partial x}. \qquad (11)$$

At the bottom boundary, a no-slip condition is imposed in the sill region and a free-slip condition is imposed in the deep region with the flat bottom. A rigid-lid approximation is used at the surface. Although the time variation of the tidal flow in the model occurs completely in phase throughout the entire domain as a result of the rigid lid approximation and the incompressibility assumption, the approximation is still valid because we are concerned only with the internal wave generation and resulting mixing over a sill with horizontal scale of ~ 100 km so that the phase of the barotropic tidal flow varies only slightly over this distance. In fact, the incoming $K_1$ tidal waves take at most 10 minutes to propagate across the sill region, much smaller than the $K_1$ period. For this reason, many previous studies such as Hibiya (1988) and Lamb (1994) successfully reproduced topographic internal wave processes using the rigid-lid approximation. To prevent artificial wave reflection at the two side boundaries, the horizontal eddy viscosity is gradually increased near the lateral boundaries up to a value of $6 \times 10^6$ cm$^2$ s$^{-1}$.

The basic vertical profiles of potential temperature and salinity (Fig. 3 ⊙) in the dataset of the U.S. National Oceanographic Data Center correspond to a summertime climatology in the Kuril Basin of the Okhotsk Sea. Crudely speaking, this stratification is thought to provide a lower estimate of the effect of tidal mixing on intermediate layer freshening because the water outflows from the Kuril Basin to the North Pacific and because salinity in the surface layer is lowest in summertime, producing a strong stratification (certainly, this is more in the realm of an educated guess). It is not particularly clear how the generation of different waves and their different propagation due to the difference in stratification would impact on the amount of mixing. With these vertical profiles, the initial stratification is set to be horizontally uniform. Model calculations start at the beginning of rightward flow (i.e., from the North Pacific to the Okhotsk Sea) so that wave generation processes can be seen clearly. According to Lamb (1994), the along-sill velocity is initialized as $v = f\sigma_f^{-1}U_0(x)$ where $U_0(x)$ and $\sigma_f$ are the maximum across-sill velocities and the frequencies of the barotropic tides, respectively.

## 3. Model results

We first describe the behavior of internal waves in one period, using an internal mode streamfunction, defined as the difference between the original solutions and the solutions obtained by setting $g = 0$. Since the solution for $g = 0$ gives the barotropic flow, which acts as the forcing (Lamb 1994), internal mode processes can be seen in terms of internal mode streamfunctions. This is not exactly true, since the $g = 0$ flow satisfies the no-slip condition at the sill by viscous effects, whereas in the full solution this boundary condition is satisfied by a combination of viscous effects and internal waves. Hence, the viscous effects are not the same in the two cases, and hence internal mode streamfunctions do not represent the true baroclinic response but also include some reminiscent effects of viscosity from the $g = 0$ case. However, since the thickness of the bottom Ekman layer [~ $(\nu_z/f)^{1/2}$] is less than 10 m in the present case, the effect of a no-slip condition is significant in only a few grids from the bottom. Thus, the current field of the $g = 0$ solution in the $K_1$ case at the time of maximum rightward flow (Fig. 4 ⊙) is vertically uniform except very near the bottom. Therefore, the baroclinic response can be fairly well described by internal mode streamfunctions.

*a. The $M_2$ case*

Figure 5 ◐▬ shows the internal mode streamfunction forced by the barotropic $M_2$ flow during the second tidal period when the initial spinup processes are almost complete. As previous studies show (e.g., Rattray et al. 1969; Baines 1982; Craig 1987), first-mode internal waves are generated on the slopes of the sill after 1.25 periods (after an interval of time corresponding to 1.25 periods) at the time of the maximum rightward flow (Fig. 5a ◐▬) and propagate away from the sill. The first-order modal waves outside of these cells were generated at the sill in the last half period and have propagated away. Wave generation on the sill slopes by rightward flow continues for up to 1.5 periods when the flow stops (Fig. 5b ◐▬), and the generated waves propagate away from the sill and reach $x \simeq \pm 60$ km after 1.75 periods. In the half period of leftward flow (Figs. 5c,d ◐▬), almost the same sequence of events can be observed, but with their phase reversed.

From Fig. 5 ◐▬, the horizontal and vertical wavelengths of the first-mode waves and the squared buoyancy frequency $N^2$ (averaged over whole depth) are about 100 km, 4 km, and $5 \times 10^{-6}$ s$^{-2}$, respectively. Using these values and the linear dispersion relation for frequency $\sigma$ and horizontal and vertical wavenumbers $k$ and $m$,

$$\sigma^2 = \frac{N^2 k^2 + f^2 m^2}{k^2 + m^2}, \tag{12}$$

the frequency of first-mode waves is estimated as $1.4 \times 10^{-4}$ s$^{-1}$, almost equal to the $M_2$ frequency. Their horizontal phase speed estimated from the dispersion relation is 2.2 m s$^{-1}$, consistent with that of 2.1 m s$^{-1}$ estimated from the figure. Thus the first-mode waves seen in Fig. 5 ◐▬ can be identified as typical internal tides at the $M_2$ frequency.

As described above, most of internal mode energy generated by the $M_2$ flow propagates away as first-mode internal tides, and dissipates gradually. In addition, since the amplitude of the barotropic $M_2$ flow is small, large-amplitude internal waves are not formed and breaking is absent. Consequently, vertical mixing induced by waves generated by the $M_2$ flow is probably not strong enough to cause significant freshening in the Kuril Straits. This is confirmed later in section 6.

## b. The $K_1$ case

The time series of the internal mode streamfunction in the $K_1$ case (Fig. 6 ◐▬) shows a quite different behavior from that of the $M_2$ case since the Kuril Straits are located north of the critical latitude for the $K_1$ tide and because the amplitude of the barotropic $K_1$ current is larger than that of the $M_2$ current. For example, sill-scale cells (cells on the scale of the sill topography) do not propagate away, and, in contrast to the $M_2$ case, intense disturbances exist on small scales.

First we describe the time evolution of the sill-scale cells. Although the $K_1$ tide is subinertial and has no characteristic curves of propagation, clockwise cells are produced on both sides of the sill after 1.25 periods (the maximum rightward flow). These cells almost vanish at the end of rightward (leftward) flow. Thus the sill-scale cells have the same frequency as the tidal frequency and do not propagate away because the $K_1$ tidal period is longer than the inertial period at the Kurils. The amplitudes of these cells are larger than those in the $M_2$ case since the barotropic flow is stronger for the $K_1$ case (note that the cell on the right-hand slope of the sill is slightly stronger than that on the left since the steeper slope produces a larger forcing of internal motion). Therefore, their effect on mixing is expected to be more vigorous and confined closer to the sill region than in the $M_2$ case. Note that problems associated with the artificial lack of $K_1$ related longitudinal radiation within a context of a two-dimensional model will be discussed later.

Next, we direct our attention to intense smaller-scale disturbances detected in Fig. 6 ◐▬. These short waves may cause considerable mixing because the process of wave breaking takes place at smaller amplitudes for waves of shorter wavelength. After 1.25 periods, the superposition of small-scale disturbances makes sill-scale cells wavy and distorted. In Fig. 6 ◐▬, such small-scale disturbances are labeled as $A_1$, $B_1$, $A_2$, $B_2$, $a_1$, and $b_1$ from left to right, with the tidal period during which they are produced indicated by subscripts and with the direction of the tidal flow at the time of their production indicated by capital (rightward) and small (leftward) letters. At the sill top, rightward flow produces disturbances $A_2$ and $B_2$. The leftward flow in the last half period has produced distortions $a_1$ and $b_1$, which are now on the right side of the sill, whereas disturbances $A_1$ and $B_1$ were produced by rightward flow in the previous period. These small-scale disturbances are clearly distinguished, as sill-scale cells disappear after 1.5 periods (Fig. 6b ◐▬). While $B_2$ stays at almost the same place, $A_1$, $B_1$, and $A_2$ move leftward, and $a_1$ and $b_1$ move rightward and are gradually dispersed. They continue to move until they reach one of the side boundaries where they then vanish. In the next half period, distortions $a_2$ and $b_2$ are produced by leftward flow and remain around the sill top until the end of the flow, in which $B_2$ at the sill top is superposed on $a_2$.

The propagation speeds of these small-scale disturbances estimated from Fig. 6 ◐▬. (0.3 ~ 1.4 m s$^{-1}$) are different from the tidal flow speed (less than 0.125 m s$^{-1}$ in the deep water region). This fact means that they are freely propagating

internal waves. Thus, their frequencies must be larger than the inertial frequency, despite that the $K_1$ frequency is subinertial.

Therefore, previous theoretical models cannot explain the generation of such intense short waves because these models assume that an oscillating tidal flow over topography can excite only internal tides corresponding to the tidal frequency. Furthermore, these features are produced by rightward (leftward) flow and propagate leftward (rightward), indicating that they move only in the upstream direction as determined at their generation time. This is also inconsistent with the character of internal tides that propagate in both directions. From these considerations, it is inferred that the intense short waves in our model must represent another class of wave. In fact, the above two qualities are characteristics of lee waves, and thus we reinvestigate the excitation mechanism of internal waves by a tidal flow in the next section to show that unsteady lee waves (which are capable of propagating away) can be excited by an oscillating flow.

## 4. The excitation mechanism of unsteady lee waves

A tidal flow over an obstacle produces vertical currents whose time variations excite internal waves. To investigate the wave excitation properly, it is necessary to consider the total time-variation of the forcing to which fluid parcels are subjected. Representing the forcing as $F$, the total time variation of the forcing $DF/Dt$ is given in Eulerian variables as

$$\frac{DF}{Dt} = \frac{\partial F}{\partial t} + U_i \frac{\partial F}{\partial x_i}, \qquad (13)$$

where $U_i$ represents the velocity of the basic flow in the $x_i$ direction. The first term on the right-hand side expresses the fact that the local time variations of forcing are capable of exciting internal waves. When the forcing is given by an oscillating tidal flow, this effect excites only internal tides of the same frequency as the basic flow. On the other hand, the second term, which represents the effect of advection, shows that the spatial variations of forcing in the frame fixed to the ground can also excite internal waves. This is because there is the temporal variation of forcing in the frame moving with the fluid at speed $U_i$ in the presence of the spatial variations of forcing in the fixed frame.

Most of the previous theories of internal waves generated by an oscillating tidal flow have neglected the advection effect in wave excitation, assuming that the tidal excursion is infinitesimal compared with the horizontal scale of the spatial variations of the forcing (i.e., a linear approximation). However, Eq. (13) shows that in regions where the tidal flow is strong and the horizontal scale of forcing is small, such as sill tops or shelf breaks, wave excitation cannot be fully taken into account unless the advection effect on wave excitation is incorporated. In fact, steady lee waves, which have quite different properties from internal tides, are generated from the advection effect as investigated in detail by atmospheric physicists (e.g., Queney 1947; Scorer 1949; Long 1953). However, the detailed dynamics of internal waves in the presence of both effects is still poorly understood. For this investigation, a description in the moving frame is appropriate to reveal the physics of internal wave excitation. Hence in the following description, frequency, phase velocity, and group velocity denote quantities in the moving frame.

To specify the nature and structure of tidally generated internal waves, we make our discussion correspond to the numerical model result performed in the vertical two-dimensional case ($\partial/\partial y = 0$). For simplicity, we assume that the flow varies as a single harmonic component of frequency $\sigma_f$ in time and that the amplitude of the topography is small in comparison with its horizontal scale; then the vertical velocity $W$ at the bottom is given by

$$W = W(x, h(x), t) = e^{i\sigma_f t} \int_{-\infty}^{\infty} \hat{W}_0(k) e^{-ikx} dk, \quad (14)$$

using a Fourier transformation. We can describe the wave forcing (14) in the neighborhood of $x = x_0$ and $t = t_0$ in the moving frame $X$ using the first-order approximation in a Taylor expansion:

$$x = X + \int_{t_0}^{t} U(x_0, t) dt \simeq X + U(x_0, t_0)(t - t_0). \quad (15)$$

This is equivalent to a local Doppler shift in time and space. Substituting this into (14) and transforming the variable $t - t_0$ to $\tau$, we obtain

$$W(x, t) = \int_{-\infty}^{\infty} \hat{W}_0(k) e^{i\sigma_f t_0} \exp[-i(kX + (kU(x_0, t_0) + \sigma_f)\tau)] dk, \qquad (16)$$

which splits into the sum of travelling waves propagating with two different phase velocities (corresponding to upper and lower signs) as

$$W(x, t) = \int_0^{\infty} \hat{W}_0(\pm k) e^{i\sigma_f t_0} \exp\{\mp i[kX + (kU(x_0, t_0) \pm \sigma_f)\tau]\} dk. \qquad (17)$$

This expression shows that the internal wave excited in the neighborhood of $x = x_0$ and $t = t_0$ by the basic flow $(U, W)$ is composed of a sum of monochromatic waves with frequency of $-kU(x_0, t_0) \pm \sigma_f$ and horizontal wavenumber of $k$. Their vertical wavenumber $m$ is determined so as to satisfy the governing equations and the condition that their energy propagates upward. The total internal wave field generated by a tidal flow over topography is formed by the superposition of these monochromatic waves excited at various times and positions.

The frequencies of the monochromatic waves consist of the term $kU(x_0, t_0)$, which arises from the spatial variation of forcing and relates to the steady lee waves, and of terms $\pm\sigma_f$, which stem from the time variation of the tidal flow and represent the internal tides. Therefore, according to the nondimensional parameter $kU_0/\sigma_f$, we can classify internal waves excited by an oscillating flow into unsteady lee waves (when $kU_0/\sigma_f \gg 1$) and "mixed tidal lee waves" (when $kU_0/\sigma_f \sim 1$), in addition to the internal tides (when $kU_0/\sigma_f \ll 1$) considered in previous theoretical models. This nondimensional parameter is a ratio of the effect of spatial to temporal forcing variations.

These three types of "topographic internal waves" have the following properties: Unsteady lee waves include classical steady lee waves in the limit of $kU_0/\sigma_f \rightarrow \infty$. Their frequencies are $-kU(t)$, and their phase velocities are $-U(t)$. Thus, unsteady lee waves can propagate in the upstream direction at their excitation time (in the upstream sense as it exists at the time of their excitation), relative not only to the fluid but also to the ground as the flow varies in time and/or space. The amplitudes of unsteady lee waves depend on the magnitude of the forcing at the time of their excitation so that the waves generated around the time of maximum flow have maximum amplitudes. Such unsteady lee waves are excited in a region where the curvature of topography is sufficiently large, such as shelf breaks. In contrast, internal tides have a frequency of $\sigma_f$ and a constant phase velocity of $\pm\sigma_f/k$, and propagate in both directions, as shown in previous studies. In the intermediate range, excited waves have intermediate properties between those of lee waves and internal tides, and we name such waves "mixed tidal lee waves."

Bell (1975) considered a similar situation to ours. However, since the waves in his treatment can be, in a sense, regarded as an infinite series of modes in the temporal domain, the unsteady lee waves and mixed tidal lee waves newly proposed here are not clearly described in his model. Consequently, his approach might be inappropriate to identify the nature of these waves. On the other hand, Lott and Teitelbaum (1993a,b) studied atmospheric lee waves using a similar approach to ours. Though they described many interesting features of unsteady lee waves, the effect of time-varying forcing on wave excitation [i.e., the first term on the right-hand side of Eq. (13)] was neglected, because tidal forcing is out of scope in most atmospheric internal waves, and hence the existence of mixed tidal lee waves could not be discussed.

In fact, consideration of the frequency of these new waves allows us to explain the reason why the subinertial $K_1$ flow can generate freely propagating internal waves at the sill top. Figure 7c  shows the distribution of vertical velocity after 0.375 period, when waves excited at the bottom around the time of maximum flow have already propagated upward. The horizontal and vertical wavelengths of the intense short wave formed at the break on the right side of the sill can be estimated as 8 km and 800 m, respectively. Accordingly, the nondimensional parameter $kU_0/\sigma_f$ becomes 5.4, indicating that the monochromatic components constituting this wave can be classed as mixed tidal lee waves but are very close to unsteady lee waves. An estimate of its frequency based on Eq. (17) yields $3.9(\pm 0.73) \times 10^{-4}$ s$^{-1}$, while an estimate based on the dispersion relation (11) becomes $4.6 \times 10^{-4}$ s$^{-1}$ using $N^2 = 2 \times 10^{-5}$ (s$^{-2}$) averaged from the surface to the sill top. The comparison shows good agreement between our theoretical model and the numerical model result. In addition, Fig. 7c  shows that the cophase lines of the internal wave generated at the right-hand break extend only in one direction, confirming that the phase of these intense short waves propagate only in the upstream direction at their generation time, with little, if any, component propagating downstream. These features are consistent with the character of unsteady lee waves.

## 5. The evolution of large-amplitude unsteady lee waves

Figures 7  and 8  show vertical velocity $(w)$ and the potential density $(\sigma_\theta)$ in the $K_1$ case, respectively, up to one period, when the generation process of the intense short waves can be seen clearly.

After 0.25 period, the barotropic $K_1$ current flows rightward with a maximum speed of 0.5 m s$^{-1}$. The vertical velocity induced by this flow is up(down)ward on the up(down)stream side of the sill, and its magnitude is larger at the sill breaks where changes in the sill slope are rapid and the horizontal flow is strong because of the shallow water around the sill top. As expected from our theoretical model, small-scale vertical velocity distributions produced at sudden changes in the sill slope generate a relatively large depression of small horizontal length at the right-hand break and adjacent weak elevation and depression over the left-hand break and sill top. These features are consistent with the intense short internal waves described in section 3b.

The displacement at the right-hand break continues to grow until the end of the rightward flow to form a large amplitude ( $\sim 100$ m) unsteady lee wave (Fig. 8d ). Similar wave growth in the decelerating stage is often observed both in field and laboratory studies (e.g., Lansing and Maxworthy 1984). On the other hand, the displacements at the left-hand break do not grow appreciably and propagate somewhat upstream as is also seen in the vertical velocity distribution. It is noteworthy that, while the lower part of the wave stays at almost the same place, the upper part propagates upstream (leftward) and the wave leans toward the upstream side. The induced cophase line of vertical velocity also tilts obliquely, indicating that modal waves

have not yet been formed. Therefore, the modal wave approximation used in the Hibiya (1986) model is not appropriate for understanding the amplification mechanism of this wave. A detailed discussion of the wave growth mechanism is given in another paper (Nakamura and Awaji 2000, manuscript submitted to *J. Phys. Oceanogr.*).

As the rightward flow vanishes after 0.5 period, the large-amplitude unsteady lee wave begins to propagate in the upstream direction at the generation time (leftward) (e.g., Fig. 7 ). Its speed of motion relative to the ground becomes faster as the barotropic flow accelerates to the left. Such propagation processes of short internal waves generated on the downstream side of a sill are consistent with observations (e.g., Farmer and Smith 1980). As the upper part of this unsteady lee wave is reflected at the surface, there appears a third modelike structure in the wave field over the sill top after 0.625 period (Fig. 7e ). Similar higher-order modal waves generated at abrupt topographic changes are often observed around shelf breaks (e.g., Kuroda and Mitsudera 1995). The correspondence with observations indicates that the processes described above are not artifacts of our numerical model but are common phenomena in real seas.

When propagating across the sill, this large amplitude wave encounters an unsteady lee wave newly generated at the left-hand break by the leftward flow (after 0.75 period). This is clearly seen in the distribution of vertical velocity (Fig. 7f ), where the propagating lee wave (a third-modelike structure) is located on the right side of downwelling associated with the new unsteady lee wave. These lee waves are superposed and interact with each other (after 0.875 period). This event produces a strong bottom-intensified current over the sill top (shown in Fig. 9 ) and a large amplitude isopycnal elevation at the foot of the unsteady lee waves after 1.0 period (above the left-hand break in Fig. 8h ).

Figure 10 shows the subsequent evolution of isopycnal displacements. As the flow turns to the right, the large amplitude elevation at the foot of the lee wave gradually breaks (density inversion is apparent in Fig. 10a ), propagating rightward, and causes vigorous vertical mixing over the sill top after 1.125 periods. As this large amplitude elevation passes over the right-hand break, it produces a strong overflow accompanied by a strong bottom-intensified current, which may strengthen the excitation of unsteady lee wave at the right-hand break (after 1.25 periods). In this superposition of newly generated and rightward propagating lee waves, the ray paths form a distinct V shape (Fig. 10c ), as in the case with internal tides. Note that unsteady lee waves can propagate only to one side in contrast to internal tides that can propagate towards both sides. The superposition of the unsteady lee waves forms a large amplitude elevation like a hydraulic jump, inducing intense vertical mixing (density inversion is apparent after 1.375 periods). Again, an unsteady lee wave grows into a large amplitude wave at the right-hand break as the barotropic $K_1$ current flows rightward (after 1.5 periods), showing that the lee wave response is not an artifact of the initial spinup of the model. In this way, large-amplitude unsteady lee waves, as shown in Figs. 8 and 10 , induce intense vertical mixing, and relatively vertically uniform water is produced over and around the sill top in the $K_1$ case.

Figure 11a shows an observed potential temperature distribution across Kruzenshterna Strait in the northern part of the Kurils where a large amplitude sill is present (Fig. 11c ). The duration time of the observation (XBT measurement by the Hokkaido National Fisheries Research Institute in Japan) is about 2.5 hours so that it roughly represents a snapshot. Comparison between the observed and modeled results is hampered by the fact that the actual sill is deeper ($\sim 950$ m) than the sill depth in the model ($\sim 550$ m) and the temperature field is influenced by the temperature difference between the Okhotsk Sea (left side) and the North Pacific (right side). However, this time series is the best available experimental dataset in this region. A conspicuous feature in Fig. 11a is the presence of large-amplitude short internal waves in the surface layer above the sill, which may cause the significant disturbance of the temperature distribution. Moreover, the elevation and depressions of isotherms around the sill suggest their presence even at mid depth. To see this more clearly, we attempted to identify the ray paths of these waves. Firstly, we applied a bandpass filter to the horizontal distribution, whose length scale roughly corresponds to a lee wave length ($2 \sim 15$ km). Then, assuming a linear relationship between the vertical displacement of isotherms ($\eta'$) and the perturbation from the basic temperature field ($\theta'$) similar to Eq. (21) (shown later), we calculated the vertical displacement from the bandpassed potential temperature. In order to avoid erroneous displacements arising from dividing by $\partial\theta/\partial z$, we derived the signal of downward and upward displacements in terms of $|\partial\theta/\partial z|\eta'$ $[\eta' \simeq -\theta'/(\partial\theta/\partial z)]$ (Fig. 11b ). In Fig. 11b , it can be seen that a ray path extends upward from close to the sill top to regions with significant wavy patterns in the surface layer, consistent with our model conclusions. As a result, we consider the possibility that unsteady lee waves are contributing to the mixing process.

## 6. Vertical mixing induced by internal waves

The numerical model results show that large amplitude internal waves produced in the $K_1$ case can cause vigorous vertical mixing over the sill. Here, we estimate the intensity of the resulting vertical mixing in terms of diffusivity. To relate the result to the parameterizations used in general circulation models, we first estimate the vertical diffusivity $K_z^E$ from an Eulerian point of view using the following Fickian formulation,

$$ K_z^E = \left| \overline{S'w'} \middle/ \frac{dS_0}{dz} \right|, \qquad (18) $$

where $dS_0/dz$ is the vertical gradient of the initial salinity profile and $\overline{S'w'}$ is salinity flux induced by perturbations, averaged over one tidal period. Figure 12 shows the estimated diffusivity using the calculated velocity fields in the second period. In the $M_2$ case, vertical diffusivity is not so large ($\sim 10$ cm$^2$ s$^{-1}$), as expected in section 3a. In contrast, the value in the $K_1$ case is very large around the sill ($\sim 10^3$ cm$^2$ s$^{-1}$) and relatively small in other regions.

However, in terms of the Fickian formulation the estimated vertical diffusivity depends fairly strongly on the vertical gradients of salinity used. Therefore, we next estimate the intensity of vertical mixing from a Lagrangian point of view. For this, we tracked numerous labeled particles in the calculated velocity field in the second period and estimated the vertical diffusivity $K^L_z$ from

$$K^L_z = 0.5 \times \frac{d\Phi}{dt} \simeq \frac{\Phi_T - \Phi_0}{2T}, \qquad (19)$$

where $\Phi$ is the variance of the particle spread, $\Phi_0$ and $\Phi_T$ are the initial (after one period) and the final (after two periods) variance, respectively, and $T$ is the tidal period (Awaji 1982). This parameter represents the apparent diffusivity due to the distortion of water particle distributions, though the value varies somewhat with the initial phase of velocity fields used in the calculation.

The estimated apparent diffusivity is shown in Fig. 13 ⊙. Vertical mixing induced by the $M_2$ current is relatively strong along the characteristic curves of $M_2$ internal tides due to the significant velocity and is widely distributed, reflecting the character of internal tides. However, its magnitude may be too small to cause the observed water modification in the Kuril Straits. In contrast, the diffusivity in the $K_1$ case is very large but concentrated near the sill. For example, the values are $\sim 10^2$ cm$^2$ s$^{-1}$ around the sill top, the maximum being of the order of $10^3$ cm$^2$ s$^{-1}$. This is mainly due to large-amplitude unsteady lee waves propagating over the sill and their superposition on unsteady lee waves newly generated by the reversed flow leading to wave breaking. Although the magnitude is smaller than that of the Fickian diffusivity, it is still much larger than that in the open oceans (about $10^3$ times larger). Because such intense vertical mixing takes place repeatedly, relatively vertically uniform water down to the depth of the density core of the NPIW ($\sigma_\theta \sim 26.8$) can be produced over and around the sill top. Indeed, after six periods, the calculated potential temperature has a relatively homogeneous distribution over the sill (Fig. 14a ⊙). Similar distributions can be found in the shallow region around the Kuril Straits (region A$_1$ in Fig. 14b ⊙), over a shallow bank just offshore of the Kruzenshterna Strait. In addition, in the Kruzenshterna Strait (region A$_2$), there are relatively fewer warm/cold patches as compared with the adjacent lateral regions. This implies the presence of relatively strong vertical mixing there, consistent with the ray path analysis described earlier. Therefore, it is suggested that vertical mixing from large-amplitude unsteady lee waves generated by the interaction of the $K_1$ current with sills is one possible mechanism contributing to the observed water modification, and in particular its refreshening in the Kuril Straits.

## 7. Energetics

It is instructive to examine the energetics of the calculated field in order to understand the energy conversion from the input $K_1$ flow to the internal waves and the subsequent intense vertical mixing described in the preceding section. In doing so, it is convenient to use the velocity field obtained from the $g = 0$ solution, $(U, V, W)$, as the barotropic flow. Since the velocity field obtained from the difference between the original solution and the $g = 0$ solution, $(u', \upsilon', w')$, gives approximately the baroclinic response, as discussed in section 3. The energy equation for the $uw$ component of kinetic energy [$\mathrm{KE}_{uw} = \rho_0(u'^2 + w'^2)/2$] is derived by multiplying Eqs. (1) and (3) by $u'$ and $w'$, respectively, and adding them together. Similarly, the energy equation for the $\upsilon$ component of kinetic energy ($\mathrm{KE}_\upsilon = \rho_0\upsilon'^2/2$) is derived by multiplying Eq. (2) by $\upsilon'$. [Note that the terms in the momentum equation for $(U, V, W)$, such as $U_t + UU_x + VU_y + WU_z$, drop out since $(U, V, W)$ is the solution for the $g = 0$ case.] The energy equation for the available potential energy (APE) is derived by multiplying the advective–diffusive equation for potential density

$$\frac{\partial \rho}{\partial t} + u\frac{\partial \rho}{\partial x} + w\frac{\partial \rho}{\partial z} = \text{dissipation} \qquad (20)$$

by $g\eta$, where $\eta$ is the vertical displacement of isopycnals. The dissipation in Eq. (20) represents an effect of diffusion terms in the equations for both potential temperature $\theta$ and salinity $S$. In the calculations, we use the linear approximation for $\eta$ and APE (Gill 1982):

$$\eta = \frac{g}{\rho_0}\frac{\rho'}{N^2}, \qquad (21)$$

$$\mathrm{APE} = \frac{1}{2}\frac{g^2}{\rho_0}\frac{\rho'^2}{N^2}, \qquad (22)$$

where $\rho'$ is the perturbation from the initial density field. Integrating over the domain with periphery $l$ (from $x = -15$ km to $x = 10$ km and from surface to 800-m depth in the sill region) using the operator $\langle \ \rangle = \iint dx\, dz$, we obtain

$$+ \langle\text{dissipation}\rangle, \tag{23}$$

$$\langle KE_v\rangle_t = C_{u\rightarrow v} + B_v + R_v + \langle\text{dissipation}\rangle, \tag{24}$$

$$\langle APE\rangle_t = C_{B\rightarrow P} - C_{P\rightarrow K} + B_{APE} + C_{N(z)}$$

$$+ \langle\text{dissipation}\rangle, \tag{25}$$

where

$$C_{B\rightarrow P} = \langle\rho'gW\rangle, \tag{26}$$

$$C_{P\rightarrow K} = \langle-\rho'gw'\rangle, \tag{27}$$

$$C_{u\rightarrow v} = \langle-\rho_0 fu'v'\rangle, \tag{28}$$

$$B_{uw} = -\oint [(u_n' + U_n)KE_{uw} + u_n'p]\, dl, \tag{29}$$

$$B_v = -\oint (u_n' + U_n)KE_v\, dl, \tag{30}$$

$$B_{APE} = -\oint (u_n' + U_n)APE\, dl, \tag{31}$$

$$R_{uw} = -\rho_0\langle u'^2 U_x + u'w'(U_z + W_x) + w'^2 W_z\rangle, \tag{32}$$

$$R_v = -\rho_0\langle u'v'V_x + v'w'V_z\rangle, \tag{33}$$

$$C_{N(z)} = -\left\langle (w' + W)APE\frac{1}{N^2}\frac{dN^2}{dz}\right\rangle. \tag{34}$$

Here, $C_{B\rightarrow P}$ is the potential energy supply from the barotropic flow. The term $C_{P\rightarrow K}$ is the energy conversion from ‹APE› to ‹$KE_{uw}$›, whereas $C_{u\rightarrow v}$ is the conversion from ‹$KE_{uw}$› to ‹$KE_v$› due to rotation effects. The quantities $u_n'$ and $U_n$ are the velocity components normal to the boundary of the domain considered; $B_{uw}$ is a boundary flux term for ‹$KE_{uw}$› with a pressure term, and $B_v$ and $B_{APE}$ are boundary flux terms for ‹$KE_v$› and ‹APE›, respectively. The terms $R_{uw}$ and $R_v$ are the Reynolds stress for the ($u'$, $w'$) and $v'$ components, respectively, and represent the kinetic energy supply from the barotropic flow. The term $C_{N(z)}$, arising from the vertical variation of $N^2$, can be interpreted as a correction term for the linear approximation of $\eta$. Adding Eqs. (23), (24), and (25) gives the temporal change of the total energy within the domain and shows that it is determined by the potential and kinetic energy supply, the boundary flux, and the dissipation.

Figure 15 ⊙ shows the temporal changes of the energy balances for ‹$KE_{uw}$›, ‹$KE_v$›, and ‹APE› up to the second tidal cycle. The value of $C_{N(z)}$ is relatively small throughout the period, showing that the linear approximation for $\eta$ works well. The energy flow responsible for the generation of internal waves is clearly seen during the spinup process in the first half period. As the barotropic flow accelerates, the potential energy supply from the barotropic flow $C_{B\rightarrow P}$ increases ‹APE› (Fig. 15c ⊙), and the resulting internal waves release their available potential energy ‹APE› into the $uw$-component kinetic energy ‹$KE_{uw}$› through the energy conversion term $C_{P\rightarrow K}$ (Fig. 15a ⊙). While most of the energy converted into ‹$KE_{uw}$› (i.e., $C_{P\rightarrow K}$) is compensated by the boundary flux $B_{uw}$, the residual can increase the value of ‹$KE_{uw}$›, and is then converted to the $v$-component kinetic energy ‹$KE_v$› by the Coriolis effect through the energy conversion term $C_{u\rightarrow v}$ (Fig. 15b ⊙). Close examination shows that $B_{uw}$ is determined primarily by the pressure term at the lower boundary (depth 800 m) of the domain defined in Eq. (29) (not shown). Since vertical velocity associated with unsteady lee waves is mostly confined above 700 m (Fig. 7 ⊙), this compensation of $C_{P\rightarrow K}$ by $B_{uw}$ may arise from a large outflux of the energy by internal tides. This in turn indicates that the net effect of internal tides on the accumulation of ‹$KE_{uw}$› is small in the sill top region. Thus, the increase of ‹$KE_{uw}$› around the sill is a direct consequence of the generation of unsteady lee waves.

After 0.5 period, the curves of the energies begin to fluctuate with a period shorter than the inertial period. This is more marked in $\langle KE_{uw} \rangle$ and $\langle KE_{\upsilon} \rangle$, and interestingly, both temporal changes are greatly influenced by the energy conversion due to rotational effects $C_{u \rightarrow \upsilon}$. Such fluctuations are attributed to the propagation of unsteady lee waves from the sill, which is clearly seen in Fig. 7 ⊙. If unsteady lee waves were trapped in the generation region, their frequency in the frame fixed to the ground is almost the same as the tidal one. In contrast, since lee waves are inertia–gravity waves, the velocity field of propagating unsteady lee waves can vary with a period shorter than the inertial period due to the Coriolis effect (i.e., $C_{u \rightarrow \upsilon}$). This result indicates that propagating lee waves as well as newly generated unsteady lee waves have a significant impact on the energy balances around the sill top.

The increase of $\langle KE_{uw} \rangle$ after about 0.75 period (and 1.75 period) in Fig. 15a ⊙ corresponds to the formation of the strong bottom-intensified current over the sill top (Fig. 9 ⊙). Figure 15a ⊙ shows that this increase of $\langle KE_{uw} \rangle_t$ also takes place through the Coriolis effect. Figure 7f ⊙ confirms unsteady lee waves passing over the sill at this moment, implying that the bottom-intensified current is produced by the lee waves. The significant energy conversion from $\langle KE_{uw} \rangle$ to $\langle KE_{\upsilon} \rangle$ and $\langle APE \rangle$ after around one period (also around two periods) is associated with the generation of large amplitude isopycnal elevation by superposition of propagating and newly generated lee waves at the left-hand break (Fig. 8h ⊙), which leads to wave breaking. After around 1.3 period, as the lee waves generated by the leftward flow propagate rightward and exit the domain, the boundary flux terms $B_{uw}$ and $B_{\upsilon}$ appreciably decrease, and the enhanced overflow at the right-hand break (Figs. 10b–d ⊙) prolongs the duration of the energy conversion from $\langle APE \rangle$ to $\langle KE_{uw} \rangle$ in the second tidal cycle as compared with that in the first cycle (Fig. 15c ⊙), thus contributing to the enhancement of internal wave fields.

The mean energy flow in the second tidal period is shown in Fig. 16 ⊙. This also indicates weak interactions between $\langle APE \rangle$ and $\langle KE_{uw} \rangle$ due to the long period of the $K_1$ tide. The temporal change of $\langle APE \rangle$ is 0.4 kJ m$^{-1}$ s$^{-1}$ on average and the net increase of $\langle APE \rangle$ is 40 MJ m$^{-1}$. Most of this large increase of $\langle APE \rangle$ is thought to be due to the formation of the relatively uniform density structure over the sill top in the model. However, the above energy equations do not include a consideration of energy radiated through the longitudinal boundaries, so that further simulations tested through detailed comparison with experimental observations are required to fully clarify the energetics in the real Kuril Straits. For example, three dimensional effects enable the $K_1$ internal tides to propagate along the isobaths (e.g., Brink 1989). In addition, the presence of vertically well-mixed water around the sill due to tidal mixing may affect the intensity of internal wave generation.

## 8. Summary and discussion

The Okhotsk Sea has been thought of as the origin of low salinity in the North Pacific intermediate layer whose manifestation is the North Pacific Intermediate Water (NPIW). In order to better understand this process, we need to clarify the mechanism responsible for the intense vertical mixing in the Kuril Straits and the associated modification of water properties, particularly the refreshening of the intermediate layer. To this end, we investigated internal waves generated through the interaction between the tidal currents (predominant in the Kuril Straits) and the sill and their effect on mixing, using a nonhydrostatic $f$-plane numerical model.

The model results reveal the following. Internal waves at the tidal frequency (internal tides) generated by the $K_1$ flow are trapped to the sill because the $K_1$ tide is subinertial in the Kuril Straits. Since the strong barotropic flow is further intensified near the bottom by the trapped internal tides, large amplitude free-propagating internal waves of short wavelengths are repeatedly generated and break around the sill top, thus producing relatively vertically uniform water over and around the sill top. On the other hand, in the $M_2$ case, most of the generated internal waves propagate away as dissipating first-mode internal tides, conveying energy away from the sill. Moreover, because the barotropic flow amplitude is small and its period is short, their amplitudes do not become so large (thus wave breaking does not occur). As a result, the $M_2$ tidal current does not have the potential to cause significant vertical mixing to explain the re-freshening in the Kuril Straits.

Our theoretical consideration identifies the large-amplitude short waves in the $K_1$ case as unsteady lee waves, whose existence has been neglected in previous oceanic internal wave theories. Because the intrinsic frequencies of unsteady lee waves are higher than the tidal frequency, the excitation of freely propagating waves (superinertial) by a subinertial $K_1$ flow is naturally explained. These unsteady lee waves, and particularly those excited at the break on the downstream side of the sill, are effectively trapped at the excitation region to form large amplitude internal waves. Furthermore, the superposition of a propagating unsteady lee wave and a newly generated lee wave over the sill generates a large amplitude internal wave, which causes wave breaking and induces intense vertical mixing over the sill top.

Although internal tides have a secondary effect on vertical mixing in the Kuril Straits at high latitudes, they are expected to induce significant vertical mixing in the subtropical and tropical regions, where the superinertial semidiurnal tides dominate. In such regions, not only unsteady lee waves but also internal tides are likely to be effectively amplified. The latter is especially so when the condition of the critical slope (e.g., Wunsch 1969) and/or the critical Froude number (Hibiya 1986) is satisfied. The combined effects of these waves are interesting problems for future theoretical and observational studies.

We estimated the vertical diffusivity from both Lagrangian and Eulerian points of view. Vertical diffusivity in the $K_1$ case

is very large around the sill in both cases, reaching a maximum value of $10^3$ cm$^2$ s$^{-1}$ in the intermediate layer and $10^1 \sim 10^2$ cm$^2$ s$^{-1}$ in the surface and deep layers. Such intense mixing occurs from the sill to the surface, reaching down to the density core of the NPIW ($\sigma_\theta \sim 26.8$). Thus it is suggested that large-amplitude unsteady lee waves generated by the $K_1$ tidal current and their breaking is one possible mechanism for the observed water modification in the Kuril Straits. In addition, the occurrence of such intense tidal mixing has the potential to explain the formation of lower temperature and higher productivity water in the Kuril Straits than the surroundings. This seems to contribute to the short ventilation time of the deep water in the Kuril Basin discussed by Riser (1996).

Since we use a vertically two-dimensional model, the subinertial $K_1$ internal tides are not properly reproduced. To examine the influence of this problem, we performed a simple numerical experiment in which the horizontal eddy viscosity and diffusivity coefficients are increased by a factor of 4 relative to those in the original case. This, in a sense, is a crude incorporation of a decrease in wave energy density as the waves propagate away, which could be caused by longitudinal wave radiation in certain cases. The result reveals that although the maximum elevation amplitude is reduced to about half of the original case due to rapid dissipation, the lee wave processes are basically the same and the estimated diffusivity is still of the order of $10 \sim 100$ (cm$^2$ s$^{-1}$). This suggests the importance of tidal mixing on the re-freshening of the intermediate layer in the actual Kuril Straits. In reality, however, the along-sill propagation of waves has a much more complex impact on wave amplitude and causes a wider range of secondary effects than can be modeled by the viscosity/diffusivity change alone.

Further modifications are required to our numerical model to approach full three-dimensionality. A flow along sills and the propagation of subinertial $K_1$ internal tides may also play an important role in water modification, for example, by transporting vertically mixed water along isobaths. Thus, quantitative estimation of the actual role of vertical mixing at the Kurils on the formation of the NPIW is beyond the power of two-dimensional model and should be investigated using a three-dimensional model. Further, wave excitation may become more complicated due to the presence of currents which flow around islands, sills, or banks. The basic state in and around the Kuril Straits is actually determined by wind-driven and thermohaline circulations, which may affect the excitation and evolution of waves. These problems are beyond the scope of the present paper and are left for future work as well as the problem of clarifying the relative importance to other processes postulated so far. Nevertheless the qualitative similarities between the observational results and our simulations point the importance of strong vertical mixing in the water modification between the Okhotsk Sea and the North Pacific.

---

**REFERENCES**

Awaji, T., 1982: Water mixing in a tidal current and the effect of turbulence on tidal exchange through a strait. *J. Phys. Oceanogr.,* **12,** 501–514.. Find this article online

Baines, P. G., 1982: On internal tide generation models. *Deep-Sea Res.,* **29,** 307–338..

Bell, T. H., 1975: Lee waves in stratified flows with simple harmonic time dependence. *J. Fluid Mech.,* **67,** 705–722..

Brink, K. H., 1989: The effect of stratification on seamount-trapped waves. *Deep-Sea Res.,* **36,** 825–844..

Bryan, K., and M. D. Cox, 1972: A numerical method for the study of the circulation. *J. Phys. Oceanogr.,* **2,** 510–514.. Find this article online

Craig, P. D., 1987: Solutions for internal tidal generation over coastal topography. *J. Mar. Res.,* **45,** 83–105..

Farmer, D. M., and J. D. Smith, 1980: Tidal interaction of stratified flow with a sill in Knight Inlet. *Deep-Sea Res.,* **27,** 239–254..

Gerkema, T., and J. T. F. Zimmerman, 1995: Generation of nonlinear internal tides and solitary waves. *J. Phys. Oceanogr.,* **25,** 1081–1094.. Find this article online

Gill, A. E., 1982: *Atmosphere–Ocean Dynamics.* Academic Press, 662 pp..

Hibiya, T., 1986: Generation mechanism of internal waves by tidal flow over a sill. *J. Geophys. Res.,* **91,** 7696–7708..

——, 1988: The generation of internal waves by tidal flow over Stellwagen Bank. *J. Geophys. Res.,* **93,** 533–542..

Kawasaki, Y., and T. Kono, 1994: Distribution and transport of Subarctic Waters around the middle of Kuril Islands (in Japanese). *Sea and Sky,* **70,** 71–84..

Kitani, K., 1973: An oceanographic study of the Okhotsk Sea—Particularly in regard to cold waters. *Bull. Far Seas Fish. Res. Lab.,* **9,** 45–77..

Kono, T., 1996: Modification processes of the intermediate subarctic water in the western North Pacific Intermediate Water. *Bull. Hokkaido Nat. Fish. Res. Int.,* **60,** 145–223..

— , and Y. Kawasaki, 1997: Modification of the western subarctic water by water exchange with the Okhotsk Sea. *Deep-Sea Res.,* **44,** 689–711..

Kuroda, Y., and H. Mitsudera, 1995: Observation of internal tides in the East China Sea with an underwater sliding vehicle. *J. Geophys. Res.,* **100,** 10 801–10 816..

Lamb, K. G., 1994: Numerical experiments of internal wave generation by strong tidal flow across a finite amplitude bank edge. *J. Geophys. Res.,* **99,** 843–864..

Lansing, F. S., and T. Maxworthy, 1984: On the generation and evolution of internal gravity waves. *J. Fluid Mech.,* **145,** 127–149..

Lee, C.-Y., and R. C. Beardsley, 1974: The generation of long nonlinear internal waves in a weakly stratified shear flow. *J. Geophys. Res.,* **79,** 453–462..

Long, R. R., 1953: Some aspects of the flow of stratified fluids, I. A theoretical investigation. *Tellus,* **5,** 42–58..

Lott, F., and H. Teitelbaum, 1993a: Topographic waves generated by a transient wind. *J. Atmos. Sci.,* **50,** 2607–2624.. Find this article online

— , and — , 1993b: Linear unsteady mountain waves. *Tellus,* **45A,** 201–220..

Nakamura, T., T. Awaji, T. Hatayama, K. Akitomo, and T. Takizawa, 2000: Tidal exchange through the Kuril Straits. *J. Phys. Oceanogr.,* **30,** 1622–1644.. Find this article online

Ohtani, K., 1989: The role of the Sea of Okhotsk on the formation of the Oyashio water (in Japanese). *Sea and Sky,* **65,** 63–83..

Queney, P., 1947: Theory of perturbations in stratified currents with application to airflow over mountains. Misc. Rep. No. 23, University of Chicago Press, 81 pp..

Rattray, M., J. G. Dworski, and P. E. Kovala, 1969: Generation of long internal waves at the continental slope. *Deep-Sea Res.,* **16,** 179–195..

Riser, S. C., 1996: Exchange of water between the Okhotsk Sea and North Pacific Ocean through the Kurile Straits. *Proc. Int. Workshop on the Okhotsk Sea and Arctic,* Tokyo, Japan, Japan Marine Science and Technology Center and Science and Technology Agency of Japan, 46–53..

Scinocca, J. F., and W. R. Peltier, 1993: The instability of Long's stationary solution and the evolution toward severe downslope windstorm flow. Part I: Nested grid numerical simulations. *J. Atmos. Sci.,* **50,** 2245–2263.. Find this article online

Scorer, R. S., 1949: Theory of waves in the lee of mountains. *Quart. J. Roy. Meteor. Soc.,* **75,** 41–56..

Talley, L. D., 1991: An Okhotsk Sea water anomaly: Implications for ventilation in the North Pacific. *Deep-Sea Res.,* **38,** S171–190..

— , 1993: Distribution and formation of North Pacific Intermediate Water. *J. Phys. Oceanogr.,* **23,** 517–537.. Find this article online

— , and Y. Nagata, 1991: Oyashio and mixed water regions as a formation area of the North Pacific Intermediate Water (in Japanese). *Sea and Sky,* **67,** 65–73..

Thomson, R. E., P. H. LeBlond, and A. B. Rabinovich, 1997: Oceanic odyssey of a satellite-tracked drifter: North Pacific variability delineated by a single drifter trajectory. *J. Oceanogr.,* **53,** 81–87..

Warner, M. J., J. L. Bullister, D. P. Wisegraver, R. H. Gammon, and R. F. Weiss, 1996: Basin-wide distributions of chlorofluorocarbons CFC-11 and CFC-12 in the North Pacific. *J. Geophys. Res.,* **101,** 20 525–20 542..

Watanabe, T., and M. Wakatsuchi, 1998: Formation of 26.8 $\sigma_\theta$ water in the Kuril Basin of the Sea of Okhotsk as a possible origin of North Pacific Intermediate Water. *J. Geophys. Res.,* **103,** 2849–2865..

Wunsch, C., 1969: Progressive internal waves on slopes. *J. Fluid Mech.,* **35,** 131–144..

Wüst, G., 1930: Meridionale Schichtung und Tiefenzirkulation in der Westhalften der drei Ozeane. *J. Cons. Int. l'Explor. Mer,* **5** (1), 21 pp..

Yasuda, I., 1997: The origin of the North Pacific intermediate water. *J. Geophys. Res.,* **102,** 893–910..

— , K. Okuda, and Y. Shimizu, 1996: Distribution and formation of North Pacific Intermediate Water in the Kuroshio–Oyashio interfrontal zone. *J. Phys. Oceanogr.,* **26,** 448–465.. Find this article online
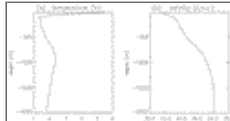
---

**Figures**
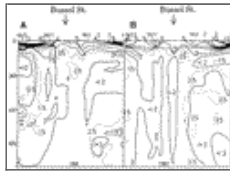
Fig. 1. Temperature sections (XBT measurements) across Bussol Strait in (a) 1991 and (b) 1992 (after Kawasaki and Kono 1994). The units are degrees Celsius.
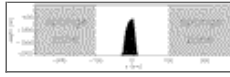
Fig. 2. The model topography, representing the vertical cross section of a strait in the northeastern part of the Kuril Islands, where tidal currents are strong enough to cause considerable mixing.

Fig. 3. Initial vertical profiles of (a) potential temperature and (b) salinity, which correspond to summer time climatology in the Kuril Basin of the Okhotsk Sea, determined from the dataset of the U.S. National Oceanographic Data Center.
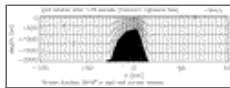
Fig. 4. Streamfunction and current vectors obtained by setting $g = 0$ in the $K_1$ case after 1.25 periods (the maximum rightward flow). The contour interval is $5.0 \times 10^5$ cm$^2$ s$^{-1}$.
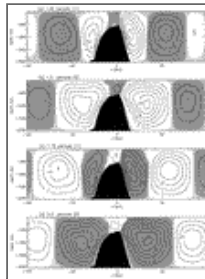
Fig. 5. The time series of the internal mode stream function in the $M_2$ case during the second tidal period after (a) 1.25, (b) 1.5, (c) 1.75, and (d) 2.0 periods. The contour interval is $1.0 \times 10^5$ cm$^2$ s$^{-1}$. Values in nonshaded areas and the thicker shaded areas are positive and negative, respectively, and the absolute values in the thinner shaded areas are less than $1.0 \times 10^4$ cm$^2$ s$^{-1}$.
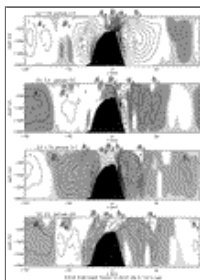
Fig. 6. Same as in Fig. 3 but for the $K_1$ case.
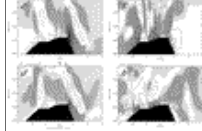
Fig. 7. The evolution of vertical velocity ($w$) in the $K_1$ case during the first period after (a) 0.125, (b) 0.25, (c) 0.375, (d) 0.5, (e) 0.625, (f) 0.75, (g) 0.875, (h) 1 period. The contour interval is 0.5 cm s$^{-1}$. Values in nonshaded areas and the thicker shaded areas are positive and negative, respectively, and the absolute values in the thinner shaded areas are less than 0.1 cm s$^{-1}$.
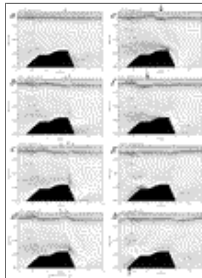
Fig. 8. The evolution of potential density ($\sigma_\theta$) around the sill top in the $K_1$ case during the first period after (a) 0.125, (b) 0.25, (c) 0.375, (d) 0.5, (e) 0.625, (f) 0.75, (g) 0.875, (h) 1 period, when the generation process of the large-amplitude unsteady lee wave can be clearly seen. For $\sigma_\theta < 26.5$, the contour interval is 0.1 $\sigma_\theta$. For $\sigma_\theta \geq 26.5$, the contour interval is 0.02 $\sigma_\theta$.
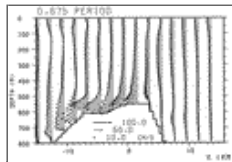
Fig. 9. The velocity vector around the sill top in the $K_1$ case after 0.875 period, when a bottom intensified current over the sill top is produced.
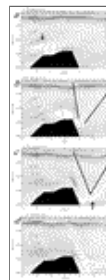
Fig. 10. The subsequent evolution of potential density ($\sigma_\theta$) around the sill top in the $K_1$ case, after (a) 1.125, (b) 1.25, (c) 1.375, (d) 1.5 periods. The contours are the same as in .
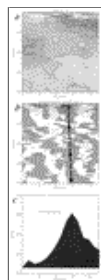
Fig. 11. (a) An observed potential temperature distribution across Kruzenshterna Strait (in 1997). Contour interval is 1°C. (b) The signal of upward (black) and downward (white) displacements of isotherms from the bandpassed potential temperature. (c) The topography in Kruzenshterna Strait.
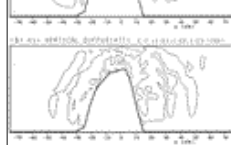
Fig. 12. Vertical diffusivity estimated from the Eulerian point of view (Fickian) for (a) the $M_2$ case and (b) the $K_1$ case, using the calculated velocity fields in the second period. Contours are logarithmic ($10^1$, $10^2$, $10^3$ cm$^2$ s$^{-1}$).
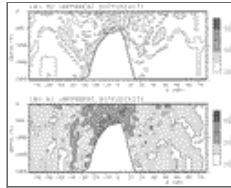
Fig. 13. Vertical diffusivity (cm$^2$ s$^{-1}$) estimated from the Lagrangian point of view for (a) the $M_2$ case and (b) the $K_1$ case, using the result of particle tracking in the calculated velocity fields for the second period.
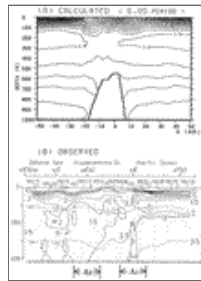
Fig. 14. (a) The calculated potential temperature distribution after six periods (contour interval is 0.2°C) and (b) the observed potential temperature distribution in Kruzenshterna Strait (A$_2$) together with a shallow bank (A$_1$), observed by the Hokkaido National Fisheries Research Institute in 1994. Dashed lines indicate isopycnal surfaces of 145, 125, and 100 cl/ton (26.6, 26.8, 27.1 $\sigma_\theta$).
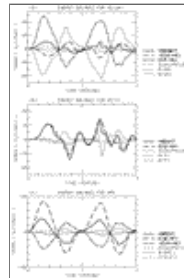
Fig. 15. The temporal change in energy balance equations for (a) ‹KE$_{uw}$›, (b) ‹KE$_\upsilon$›, and (c) ‹APE› in the $K_1$ case. Terms in the figures are defined in Eqs. (23) through (34).
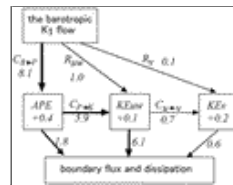
Fig. 16. The energy flow diagram time-averaged over the second cycle in the $K_1$ case. Terms in the figures are defined in Eqs. (23) through (34). The values are in units of kJ m$^{-1}$s$^{-1}$.

*Corresponding author address:* Dr. Tomohiro Nakamura, Department of Geophysics, Kyoto University, Kyoto 606 8502, Japan.

E-mail: nakamura@kugi.kyoto-u.ac.jp